Dalton Transactions

PAPER

View Article Online
View Journal | View Issue

Cite this: *Dalton Trans.*, 2015, **44**, 7477

Synthesis and aggregation behaviour of luminescent mesomorphic zinc(II) complexes with 'salen' type asymmetric Schiff base ligands

Sutapa Chakraborty,[a] Chira R. Bhattacharjee,*[a] Paritosh Mondal,[a] S. Krishna Prasad[b] and D. S. Shankar Rao[b]

Received 24th December 2014,
Accepted 10th March 2015

DOI: 10.1039/c4dt03989k

www.rsc.org/dalton

A new series of photoluminescent Zn(II)-salen type asymmetric Schiff base complexes, [ZnL], H_2L = [*N*,*N*′-bis-(4-*n*-alkoxysalicylidene)-1,2-diaminopropane] (*n* = 12, 14 and 16) have been accessed and their mesomorphic and photophysical properties investigated. Though the ligands are non-mesomorphic, coordination to Zn^{2+} ion induces liquid crystalline behaviour. The complexes exhibited a lamello-columnar phase (Col_l) as characterized by a variable temperature powder X-ray diffraction (XRD) study. Intense blue emissions were observed for the complexes at room temperature in solution, in the solid state and in the mesophase. Aggregation properties of the complexes were explored in different solvents through absorption and photoluminescence studies. While de-aggregation to monomers occurred in coordinating solvents due to axial coordination to Zn(II), aggregates were formed in the solution of non-coordinating solvents. Density functional theory (DFT) computation carried out on a representative complex using a GAUSSIAN 09 program at the B3LYP level suggested a distorted square planar geometry. The results of a time-dependent DFT (TD-DFT) spectral correlative study showed the electronic properties of the complex molecule to be in compliance with the spectral data.

1. Introduction

Transition metal–salen complexes have been a recurrent theme in synthetic co-ordination chemistry, yet interest in this field continues unabated, possibly due to their wide applicability being unfolded in recent times.[1–4] A plethora of salen based complexes are now known to act as efficient catalysts both in homogeneous and heterogeneous reactions for asymmetric ring-opening of epoxides, aziridination, cyclopropanation, oxidation, reduction reaction of ketones, epoxidation of olefins, formation of cyclic and linear polycarbonates, catalytic enantioselective and diastereoselective redox reactions and Diels–Alder reactions.[5–8] Metal salen complexes are also efficient entities to study interactions with DNA, leading to the development of sensitive chemical probes for DNA.[9–12] Besides, such systems are also known to exhibit interesting fluorescence,[13–17] magnetic,[17,18] non-linear optical[19–21] and liquid crystalline properties[22–30] and act as electrochemical sensors.[31–33] Metallomesogens based on Zn(II)-salen complexes are quite intriguing because of the possibility of combining luminescence with liquid crystallinity to generate newer systems with exotic multifunctional properties.[34–37] Spacer group modification can lead to substantial changes in mesophase as well as photophysical behavior in such hemi-disc shaped complexes.[34–37] In the past few years we have reported some novel fluorescent liquid crystalline Zn(II)-salen complexes with different spacer groups showing hexagonal, rectangular and rectangular/oblique columnar mesomorphism.[35–37] By creating a minor modification at the central aromatic ring (spacer), new symmetry as well as newer organization in the mesophase could be achieved.[35–37]

Zn(II)-salen complexes and their derivatives also facilitate various structures which may be utilized in sensory materials for the detection of alkaloids[38] and nitro aromatics,[39,40] in the recognition of biologically relevant anions,[41] in selective receptors for tertiary amines,[42] in self-assembled heteromultimetallics,[43,44] in supramolecular box-shaped assemblies,[45,46] in molecular templates in catalytic studies,[47,48] in dopants for high performance OLEDS[49–51] and in the exploration of their unique second-order nonlinear optical properties.[19,20] The high Lewis acidity of the co-ordinatively unsaturated Zn^{2+} ion is believed to be the key to such behavior. The pentacoordinate nature of the Zn^{2+} ion boosted by the rigid geometry of the salen framework facilitates the axial binding of donor ligands, resulting in substantial variations in the optical absorption

[a]*Department of Chemistry, Assam University, Silchar 788011, Assam, India. E-mail: crbhattacharjee@rediffmail.com; Fax: +91-03842-270342; Tel: +91-03842-270848*
[b]*Centre for Nano and Soft Matter Sciences, Jalahalli, Bangalore 560013, India*

behaviour and enhanced fluorescence emission. In the absence of an axial ligand, coordinative saturation is achieved through intermolecular Zn···O interactions involving the phenolate oxygen atoms of the salen ligand acquiring a square based pyramidal structure.[52,55]

In continuation of our pursuit of designing photoluminescent metallomesogens, we report herein a new series of Zn(II) complexes of asymmetric 'salen' based *N*,*N*′-bis-(4-*n*-alkoxysalicylidene)-1,2-diaminopropane ligands. Induction of mesomorphism and photoluminescence *via* coordination to Zn(II) ion has been demonstrated. All the complexes are blue light emitters both in the solid state as well as in solution. The complexes all exhibited aggregate formation in non-coordinating solvents while only a monomer is favoured in coordinating solvents. Density functional theory (DFT) calculations carried out using the GAUSSIAN 09 program at the B3LYP level revealed a distorted square planar geometry around the metal center in the complexes. A time-dependent DFT spectral correlative study was undertaken to account for the electronic transitions in the complexes.

2. Results and discussion

2.1. Synthesis and structural assessment

Condensation of 4-alkoxy substituted aldehyde with the unsymmetrical amine, 1,2-diamino propane afforded the 'salen' type asymmetric Schiff base ligands. The strategy implemented for the synthesis of Schiff base ligands, [*N*,*N*′-bis-(4-*n*-alkoxysalicylidene)-1,2-diaminopropane], hereafter abbreviated as ***n*dap** (*n* = 12, 14 and 16 is the number of carbon atoms in alkyl chains; dap = 1,2-diaminopropane) and the mononuclear complexes (**Zn-*n*dap**) is summarized in Scheme 1. The structures of the ligands and the corresponding Zn(II) complexes were probed by elemental analyses, UV-visible, FT-IR and ^{1}H NMR spectroscopy. A broad band at ~3370 cm^{-1} attributed to the phenolic –OH group is observed in the FT-IR spectra of the ligands (***n*dap**). The C=N stretching vibration of the ligands are located in the region of 1653–1655 cm^{-1}. Upon complexation, the shift of the $\nu_{C=N}$ mode to a lower wave number, ~1638 cm^{-1} ($\Delta\nu \approx 16$ cm^{-1}) and the absence of a ν_{O-H} mode attest to the deprotonation of the Schiff-base prior to coordination of azomethine nitrogen and phenolate oxygen to the Zn^{2+} ion. The ^{1}H NMR spectra of the ligands showed two characteristic signals, at δ = 11.45 ppm, corresponding to the OH proton, and at ~8.22 and 8.18 ppm due to the resonance of two asymmetric imine protons. The ^{1}H NMR spectra of the corresponding Zn(II) complexes did not exhibit any signal for the phenolic –OH proton. Additionally, an upfield shift (~0.56 ppm) in the peak position of the –N=CH protons further validated azomethine nitrogen coordination.

2.2. Mesomorphic study

The mesophase behaviour of the compounds has been investigated by polarizing optical microscopy (POM), differential scanning calorimetry (DSC) and variable temperature powder XRD techniques. Free ligands (***n*dap**) are non-mesomorphic, presumably owing to greater conformational flexibility. However, upon complexation with a Zn(II) metal ion, mesomorphism is induced due to enhanced rigidity of the Schiff base ligand framework. The phase sequence, transition temperatures and associated enthalpies for the Zn(II) complexes are presented in Table 1. The complexes all exhibited enantiotropic liquid crystalline behavior. On cooling from the isotropic melt, a grainy texture was observed at 125 °C (Fig. 1). The DSC thermogram of the complexes **Zn-14dap** and **Zn-16dap** (Fig. 2) exhibited two transitions, each in the heating and cooling cycle. In the cooling scan, the grainy texture at the mesophase remains unaltered till ambient temperature, slowly freezing into a glassy state. For the **Zn-12dap** complex, two additional peaks observed in the heating cycle were ascribed to crystal–crystal transitions. No isotropic liquid-mesophase transition

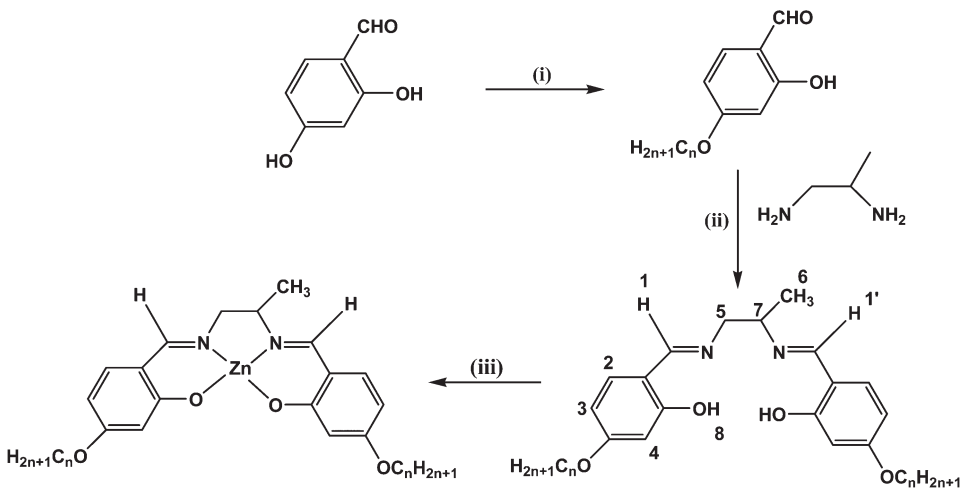

Scheme 1 (i) $C_nH_{2n+1}Br$, $KHCO_3$, KI, dry acetone, Δ, 24 h, (ii) glacial AcOH, absolute EtOH, Δ, 3 h and (iii) $Zn(OAc)_2{\cdot}2H_2O$, MeOH, stir, 3 h.

Table 1 Thermodynamic data for the **Zn-*n*dap** (n = 12, 14, 16) complexes. Transition temperatures are given in °C, and the corresponding enthalpy changes are in parentheses (ΔH; kJ mol^{-1}). Cr, Cr_1, Cr_2 refer to phases that are crystalline or solid; Col_l: lamello-columnar phase

Compounds	Heating[a]	Cooling[a]
Zn-12dap	Cr 94.1 (32.8) Cr_1 103.4 (2.4) Cr_2 134.5 (7.9) Col_l 168.6 (1.5) I	I 83.7 (10.1) Cr
Zn-14dap	Cr 97.6 (7.9) Col_l 167.4 (14.1) I	I 144.9 (12.2) Col_l 92.2 (6.3) Cr
Zn-16dap	Cr 98.5 (7.0) Col_l 162.1 (8.2) I	I 124.2 (6.2) Col_l 90.3 (5.9) Cr

[a] DSC peak temperature.

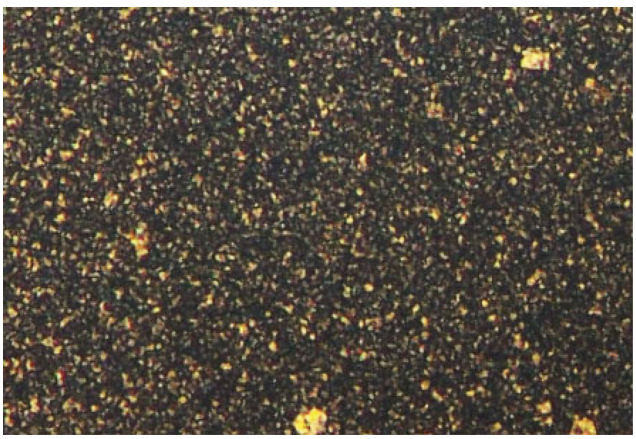

Fig. 1 POM image of **Zn-16dap** upon cooling at 125 °C.

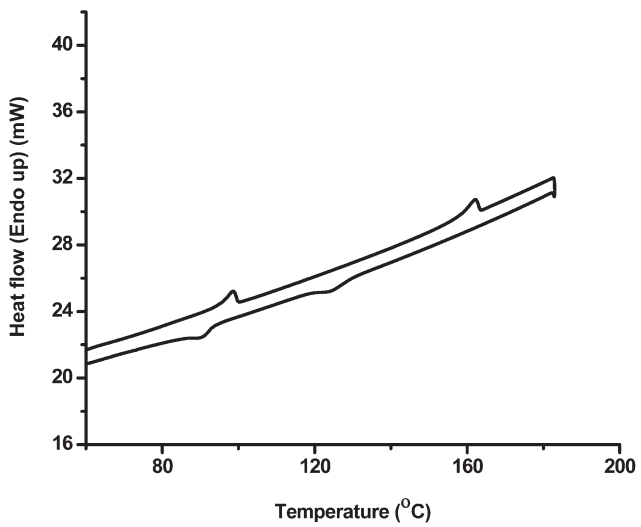

Fig. 2 DSC profile of **Zn-16dap**.

could be detected in the cooling cycle (Table 1). This might be due to the partial vitrification of the mesophase. Viscous nature of the complexes tends to affect the molecular mobility causing a pronounced hysteresis in the phase transition temperature in all the cases. A gradual decrease in the clearing temperature was observed with increasing number of carbon atoms in the pendant alkoxy arm. The isotropic liquid to mesophase transition temperature also displayed similar trends with increasing chain length. Repeated heating and cooling scans confirmed the reversibility of the thermal behaviour.

Variable temperature powder XRD study of a representative complex, **Zn-16dap** was carried out both in the mesophase and at room temperature. The X-ray diffraction pattern recorded at 100 °C (Fig. 3a, Table 2) contained several sharp and intense Bragg reflections in the small-angle region and two broad scattering halos (visualized by profile fitting of the data) in the wide-angle region. The broad maxima centered around 4.7 Å and 4.0 Å correspond, respectively, to the lateral short-range order of the molten chains and the molecular cores, confirm-

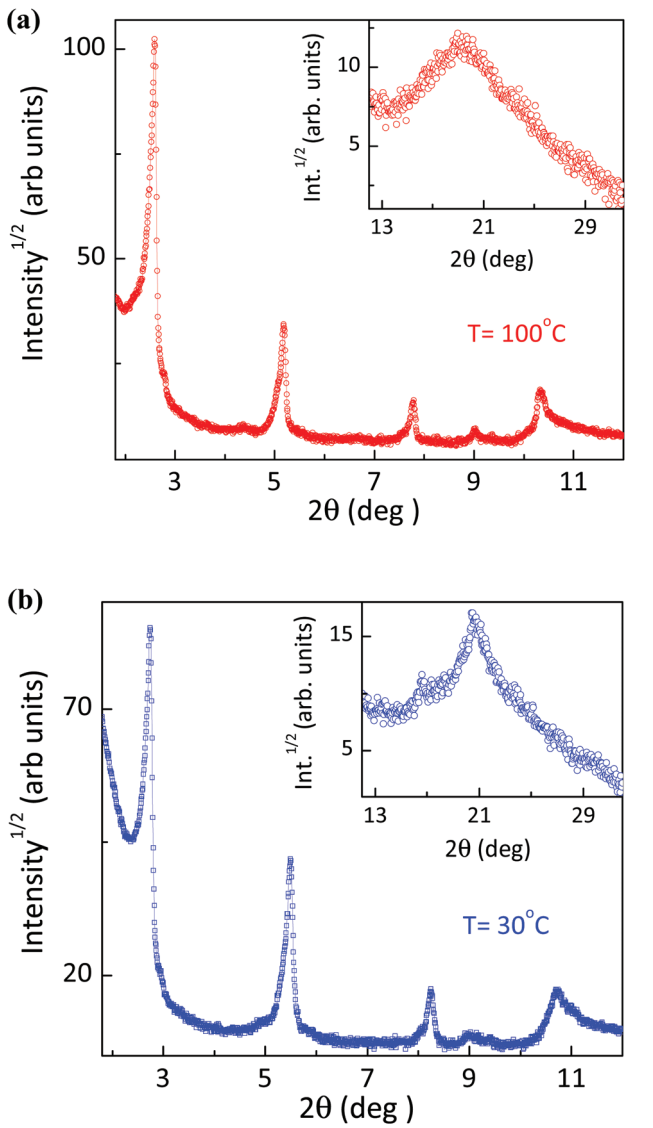

Fig. 3 PXRD pattern of **Zn-16dap** at (a) 100 °C and (b) at room temperature (30 °C).

Table 2 PXRD data of **Zn-16dap**

Temperature (°C)	Parameters	d_{meas} [a,b]/ Å	$d_{calc.}$ [a,b]/ Å	Miller indices (hkl)[c]
At 100 °C	a = 34.06 Å	34.05[s]	34.06	100
	b = 40.46 Å	17.06[s]	17.03	200
	V_{cell} = 5540.5 Å^3	11.37[s]	11.35	300
	d = 34.1 Å	9.81[s]	9.70	140
		8.54[s]	8.70	240
		4.68[d]		
		4.02[d]		
At 30 °C	a = 32.18 Å	32.19[s]	32.18	100
	b = 41.31 Å	16.10[s]	16.09	200
	V_{cell} = 5596.5 Å^3	10.72[s]	10.73	300
	d = 32.18 Å	9.87[s]	9.83	140
		8.24[s]	8.26	050
		7.87[s]	7.90	410
		6.51	6.55	350
		5.72	5.76	450
		5.32	5.32	610
		4.29[d]		
		4.21[d]		

[a] $d_{meas.}$ and $d_{calc.}$ are the experimentally measured and calculated diffraction spacing, respectively. [b] Intensity of the reflections: s; sharp peak, d: diffuse peak. The distances are given in Å. [c] [hkl] are the Miller indices of the reflections. For Col_l phase, $d = (\sum ld_{l00})/N_{l00}$ where N_{l00} is the number of reflections. V_{cell}, is the unit cell volume.

ing the liquid nature of the mesophase. The sharpness of the small-angle reflections indicates long-range correlation of the structure. However, these reflections do not conform to either a purely lamellar or purely columnar structure. The first three reflections (at 34.1, 17.1 and 11.4 Å) being in the reciprocal spacing ratio 1 : 2 : 3, point to a well-defined layered structure. In contrast the remaining two sharp reflections observed at 9.8 Å and 8.5 Å cannot be ascribed to a lamellar form, but can be explained by invoking a columnar ordering. Since these peaks are much less intense than the primary layer peak, they can be considered to be arising due to 2-D columnar modulation of the layers. A mesophase exhibiting structural features which are a combination of the lamellar and columnar features has been referred to as a lamello-columnar (Col_l) phase.[24,26–28,30] Symmetric 4-alkoxy substituted Schiff bases containing ethylene diamine spacer complexed to Pt^{2+}, Cu^{2+}, VO^{2+} and Ni^{2+} have also been shown to exhibit Col_l phases though the 1D ordering is more pronounced in these cases.[24,27,28,30] Though the corresponding Zn(II) complexes have been documented, the mesomorphic properties have not been reported.[52] The low intensity for second wide-angle halo expected due to interaction between the rigid part of one mesomorphic unit and its next nearest neighbour suggests weaker correlation between the cores within the column in the mesophase. The enhanced flexibility associated with the aliphatic spacer group bearing the 'methyl' substituent is believed to induce bending and twisting deformations, with the resulting fluctuations reducing the core–core correlations.[56,57] Similar behaviour has also been noticed for previously reported analogous Zn(II) and Cu(II) complexes with asymmetric methyl substituted aromatic spacer.[22,37]

Spacer group substitution can have marked influence on the mesomorphic properties in the 'salen type' zinc(II) complexes. In our previous reports[35–37] on zinc(II)-salen complexes, the effect of different substituents at the aromatic spacer (X = H, CH_3, Cl *etc.*) were studied and the complexes were shown to exhibit hexagonal, rectangular and oblique columnar mesophases of different symmetries. While complexes without any substituent or with an electron donating methyl group at the aromatic spacer exhibited monotropic phase behaviour, the electron withdrawing substituent (Cl) at the spacer stabilized the mesophase and enantiotropic phase behaviour was observed. Enhanced dipolar interactions due to the electron withdrawing group has been argued in favour of better core–core correlations with an increase in the clearing temperature than analogous compounds with methyl or without any substituent.

The XRD spectrum recorded at 30 °C (Fig. 3b) was quite similar to that recorded at high temperatures. However, the diffractogram consisted of additional reflections which agree with the assignment of the Col_l phase; the presence of diffuse reflections at wide angles and the absence of any mixed-index reflections at low angles rules out the phase being crystalline in nature at this temperature. Further, the core–core peak becomes much stronger. Inserting the full width at half-maximum value of this reflection in the standard Scherer equation yields a correlation length of about 115 Å, associated with the stacking of about 28 molecules along the columns. It may also be mentioned that the calculated inter-layer distance in the mesophase, d = 34.1 Å, is greater than the DFT computed radius (~23.9 Å) of the fully extended half-disc shaped molecule. Though additional information regarding the stacking of the molecular cores in the mesophase is not available, it is presumed that the half-disc shaped molecules might perhaps preferably arrange themselves in an anti-parallel partially interdigitated manner within the layer (Fig. 4).[56,57]

2.3 Photophysical properties

The UV-visible absorption and photoluminescence spectra of the compounds recorded in chloroform, $CHCl_3$ (2×10^{-5} M) at room temperature are shown in Fig. 5a and b and the data are

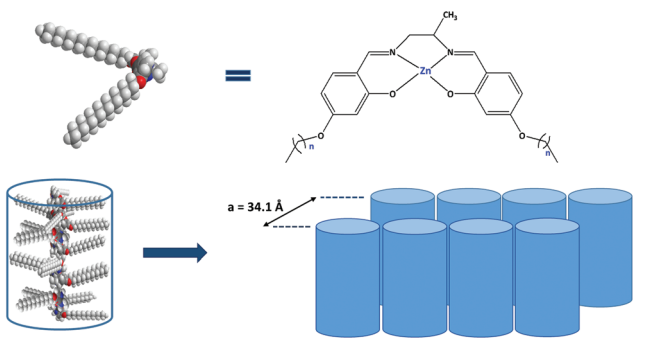

Fig. 4 Anti-parallel interdigitated organization of the molecules in lamello-columnar phase.

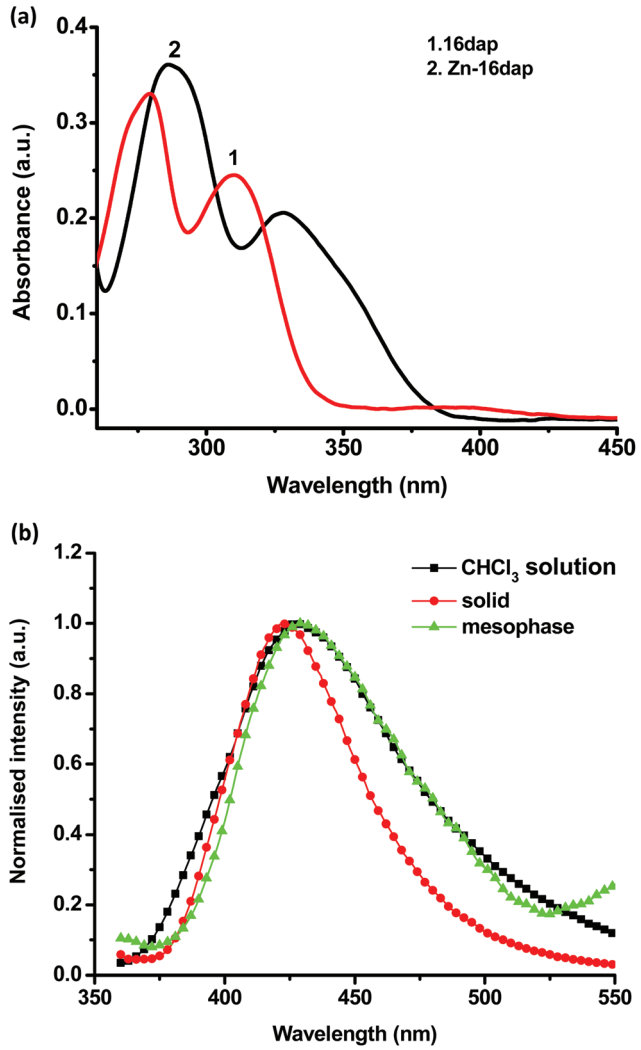

Fig. 5 (a) UV-visible absorption spectra of the ligand (**16dap**) and **Zn-16dap** in chloroform (2×10^{-5} M) and (b) intensity (normalized) *vs.* wavelength photoluminescence profile for the **Zn-16dap** complex in chloroform solution (2×10^{-5} M), solid state and in mesophase ($\lambda_{ex.}$ = 330 nm).

Table 3 UV-visible and photoluminescence spectral data of the ligands (in $CHCl_3$) and **Zn-*n*dap** (*n* = 12, 14, 16) complexes in different solvents

Compounds	Solvents	Absorption λ_{max} (nm)	Absorption ε (l mol^{-1} cm^{-1})	Emission λ_{max} (nm)
12dap	$CHCl_3$	278	16 312	—
		310	12 300	
		386	192	
14dap	$CHCl_3$	278	15 936	—
		310	12 305	
		386	200	
16dap	$CHCl_3$	279	16 530	—
		310	12 296	
		386	174	
Zn-12dap	$CHCl_3$	287	20 359	425
		330	11 240	
		345^{sh}	7875	
	CH_2Cl_2	286	28 967	424
		331	16 543	
		345^{sh}	12 756	
	Toluene	287	16 748	421
		333	10 731	
		346^{sh}	8156	
	THF	288	31 952	432
		345	23 675	
		360^{sh}	18 789	
Zn-14dap	$CHCl_3$	287	19 935	425
		330	10 306	
		347^{sh}	7693	
	CH_2Cl_2	286	28 733	424
		331	16 238	
		347^{sh}	13 085	
	Toluene	287	16 892	422
		333	10 736	
		346^{sh}	9712	
	THF	288	31 132	433
		345	22 925	
		361^{sh}	19 003	
Zn-16dap	$CHCl_3$	287	20 135	425
		329	10 240	
		343^{sh}	7675	
	CH_2Cl_2	286	29 784	424
		331	16 998	
		346^{sh}	12 985	
	Toluene	286	16 998	421
		333	10 706	
		345^{sh}	8215	
	THF	288	32 082	432
		345	23 405	
		359^{sh}	18 715	

sh: shoulder.

summarized in Table 3. The UV-visible absorption spectra of the ligands (***n*dap**; *n* = 12, 14, 16) consisted of two intense absorption bands centered at ~278 and ~310 nm, attributed to the π–π* transition localized on the aromatic rings (Fig. 5a). Another less intense band at ~386 nm may be attributed to n–π* excitation of the C=N fragment. Upon complexation, the former two bands were red-shifted to ~287 and ~329 nm, respectively, with the appearance of an additional shoulder at ~346 nm, while the low intensity band due to the n–π* transition in the ligand disappeared because of the participation of the nitrogen's lone pair in coordination to the Zn^{2+} ion. The photoluminescence spectra of the ligands and Zn(II)–salen complexes were recorded at room temperature in $CHCl_3$ solution (2×10^{-5} M), mesophase and also in the solid state (Fig. 5b). The ligands are non-emissive. The solid state emission spectra of the complexes were recorded by placing a uniform powder sheet between two quartz plates. The complexes showed a blue luminescence with emission maxima centered at ~424 nm and an emission quantum yield of ~23% (solution), and ~5% (solid) under UV irradiation (330 nm). The observed fluorescence emission originates from metal-perturbed π–π* ligand-centered transitions. With respect to solution, the position of the emission maxima is virtually unaltered in the solid state. However, the emission intensity quenches substantially following closer association of molecular cores in the solid state as compared to the solution. In a POM study, the mesophase of the Zn(II) complex that was developed at 125 °C during the cooling cycle freezes into a glassy state persisting till ambient temperature enabling photoluminescence study in the mesophase ($\lambda_{max} \approx 425$ nm) as well.

Similar studies in the frozen glassy state were made earlier for related complexes.[34] The emission energies are virtually unaffected in the solid state, in solution and in the mesophase (Fig. 5b).

Notably, the nature of substituent also has marked influence on the emission behavior of such complexes. When compared to systems with methyl or un-substituted aromatic spacer group, a distinct red shift (~40 nm) of the emission band has been noticed on going from the un-substituted zinc(II) complex to the chloro-substituted one.[35–37] This is believed to arise from the electron withdrawing effect of the chloro group on the π–π* transition of the corresponding complex. The observed photophysical behaviour is consistent with those reported for Zn(II) complexes of Schiff bases substituted with electron donating/withdrawing groups.[58] Emission maxima of complexes with differently substituted (X = H, CH_3, Cl) aromatic spacers studied earlier[35–37] were observed at >500 nm. In the present case of methyl substituted aliphatic bridges, the emissions were significantly blue shifted to ~424 nm consistent with the enhanced flexibility.

UV-visible and photoluminescence spectra of the Zn(II)-salen complexes (Fig. 6a and b) were also recorded in dilute solutions (2×10^{-5} M) of different coordinating and non-coordinating solvents in order to study the de-aggregation/aggregation phenomena. The absorption spectra recorded in non-coordinating solvents (*e.g.* CH_2Cl_2, $CHCl_3$ and toluene) consisted of two well-defined bands located at ~287 nm, 331 nm and a shoulder at 345 nm (Fig. 6a) attesting the formation of aggregates.[53,54] In coordinating solvent (THF), a red shift (~14 nm) of the longer wavelength feature is observed due to the axial coordination of the solvent molecules, suggesting de-aggregation (Fig. 6a).[53,54] The coordinatively unsaturated Zn^{2+} ion behaves as a Lewis acid. This behavior is unlike that observed in the case of the symmetrical molecule containing an ethylene diamine spacer wherein upon de-aggregation a blue shift of longer absorption feature was noticed.[52] A rather unusual optical behavior is attributed to the lack of conjugation between the J-type aggregated salen moieties. The methyl group being electron donating in nature induces a considerable amount of conjugation (+I effect) in the ligand framework in the present complexes. Also the tetrahedral methyl group, due to its steric requirement, tends to restrict the salicylidene groups of each unit in the dimer to H-type aggregate (Fig. 6c). Similar results were obtained in other related systems with conjugated aliphatic and aromatic spacers.[53,54] Concentration variations had virtually no effect on these features up to a concentration of 1×10^{-4} M (Fig. 7). Photoluminescence spectra of the complexes (Fig. 6b) recorded in non-coordinating solvents exhibited a broad band at ~424 nm. In coordinating solvents, the maxima is slightly red shifted (~8 nm) with enhancement in fluorescence intensity suggesting de-aggregation with concomitant formation of 1 : 1 adduct.[53,54] The emission quantum yield values in non-coordinating solvents (*e.g.* CH_2Cl_2, $CHCl_3$ and toluene) are around 22% which were enhanced (EQY = 38%) upon de-aggregation in coordinating solvent. Fluorescence of face-to-face-stacked

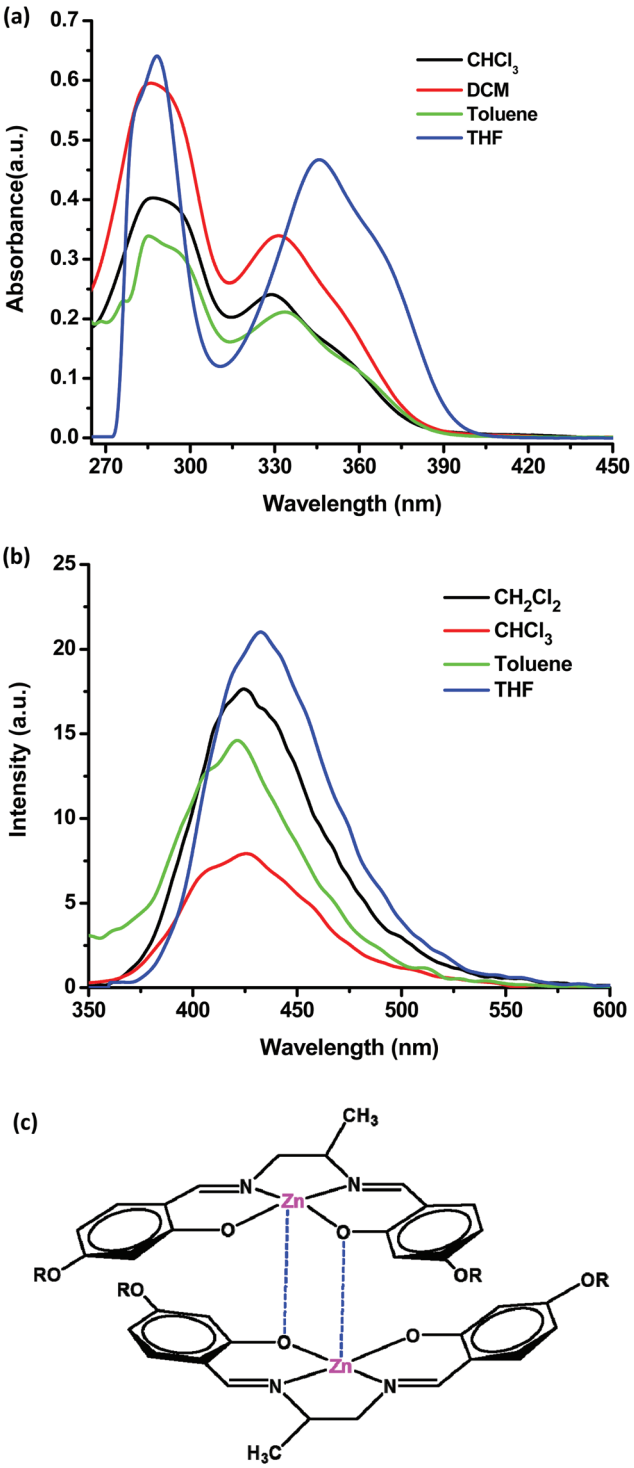

Fig. 6 UV-visible absorption spectra (a), fluorescence spectra (λ = 330 nm; with 10% attenuator) (b) of **Zn-16dap** (2×10^{-5} M) in different non-coordinating and coordinating solvents and (c) the 'H-type' dimer in solution of non-coordinating solvents.

H-type dimer aggregates (sandwich-type dimers) are known to be quenched relative to that of the monomer.[59] A rapid energy relaxation of the lower excited states causes this fluorescence

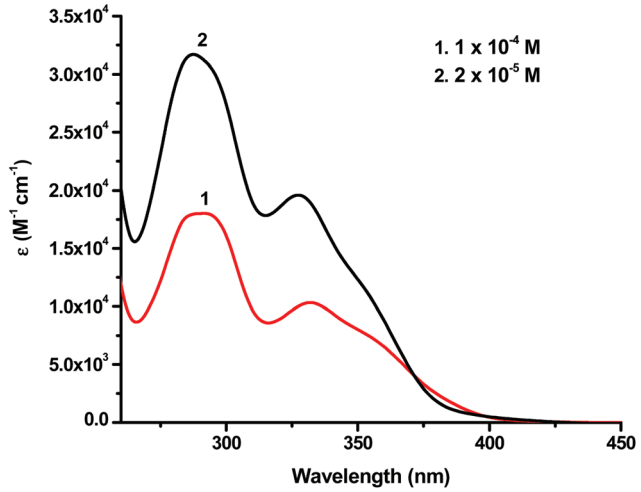

Fig. 7 Concentration dependence of UV-visible absorption spectra of **Zn-16dap** in $CHCl_3$ solutions.

suppression. The absorption or emission characteristics of the complexes are invariant of the alkyl chain lengths (Table 3).

In order to minimize inter-electronic repulsions, Zn(II) ion prefers a tetrahedral geometry to a square planar coordination. However, a short rigid central spacer with steric demands in the present complexes forces the metal center to acquire an unfavourable distorted planar geometry which eventually lead to a dimer, $[ZnL]_2$ [60] instead of more stable helical shape formed by tetrahedral 2 : 2 metal-to-ligand complex, $[Zn_2L_2]$.[61]

2.4. DFT study

In the absence of diffraction quality single crystals, density functional theory (DFT) calculations were carried out on a representative Zn(II) complex (**Zn-16dap**) employing a GAUSSIAN 09 program package[62] to arrive at the optimized electronic structure. The ground state geometry optimization in the gas phase of the zinc complex has been performed using the three-parameter fit of Becke's hybrid functional combined with the Lee–Yang–Parr correlation functional termed a B3LYP hybrid,[63,64] generalized gradient approximation (GGA) exchange along with 6-311+G(d,p), 6-31+G(d,p), 6-31G(d) and 6-31G basis sets[65] for Zn, N and O, C and H, respectively, without imposing any symmetry constraint. The appropriate structure of the complex was confirmed as energy minima by calculating the vibrational frequency and confirming the absence of any imaginary frequencies. Based on the optimized geometry of the zinc complex, TD-DFT calculations on an isolated molecule of the title complex (**Zn-16dap**) have been performed at the B3LYP level to study the spectroscopic and electronic properties. Since the electronic absorption spectra of the compounds were recorded in dichloromethane, the solvent effects were taken into consideration in the theoretical modelling. The GAUSSSUM[66] program was employed to calculate the individual contribution of various groups to each molecular orbital. A solvation method of the polarisable continuum model (PCM)[67] using the integral equation formalism (IEF) variant[68] was considered in the calculations. Important geometric parameters of the optimized Zn(II) complex as evaluated by DFT at the B3LYP level are collected in Table 4. Average Zn–O and Zn–N bond lengths of the Zn(II) complex are calculated to be 1.931 and 2.077 Å, respectively. The O1–Zn–O2 and N1–Zn–N2 bond angles are found to be 108.9° and 80.0°, respectively. The O1–Zn–N1, O2–Zn–N2, O1–Zn–N2 and O2–Zn–N1 bond angles are calculated to be 91.9°, 92.1°, 148.6° and 148.8°, respectively, around the zinc atom indicating a distorted square planar geometry (Fig. 8). The dihedral angle O1–N3–N2–O2 as evaluated from DFT calculation is about 39.7° reflecting a deviation from planarity.

The three-dimensional (3D) iso-surface plots of the lowest unoccupied molecular orbitals (LUMOs) and the highest occupied molecular orbitals (HOMOs) of the zinc complex are presented in Fig. 9. The electron density of the HOMO is localized almost entirely on the aromatic rings, while that of the LUMO is mainly centered on both N=C bonds and aromatic rings. The HOMO and LUMO energies are calculated to be −5.58 eV and −1.41 eV, respectively, the energy difference being ΔE = 4.17 eV. This value is somewhat higher than the HOMO–LUMO energy difference value (ΔE = 3.60 eV) evaluated from the lowest energy UV-Vis band (346 nm). Extensive intermolecular interactions in the solution phase (UV-Vis study) as against a free gaseous molecule (DFT study) could be one plausible reason for such a deviation. While ligand p_π orbitals contribute almost entirely to HOMO−1 (98%), HOMO−2 (99%), HOMO−3 (100%) orbitals, the HOMO−4 orbital receives a negligible contribution from metal d_π orbitals (8%). Electron density on LUMO+1, LUMO+3 and LUMO+4 orbitals is mainly due to ligand p_π* orbitals while that on LUMO+2 is primarily due to metal d_π* orbitals (87%).

TD-DFT calculations have been carried out for the **Zn-16dap** complex to account for the observed bands in the UV-visible region. The key electronic transitions, corresponding oscillator strength (f), orbitals involved in these transitions and their percentage contribution to each transition are summarized in Table 5. The surface of each peak in the spectra is proportional to oscillator strength (f), which also reveals the probability of

Table 4 Selected bond lengths (Å) and bond angles (°) of **Zn-16dap** complex optimized at the B3LYP level

Structural parameter	Bond lengths (Å) and bond angles (°)
Zn–O1	1.932
Zn–O2	1.931
Zn–N1	2.076
Zn–N2	2.078
O1–Zn–O2	108.9
N1–Zn–N2	80.0
O1–Zn–N1	91.9
O2–Zn–N2	92.1
O1–Zn–N2	148.6
O2–Zn–N1	148.8
O1–N1–N2–O2	39.7
Molecular length	47.8

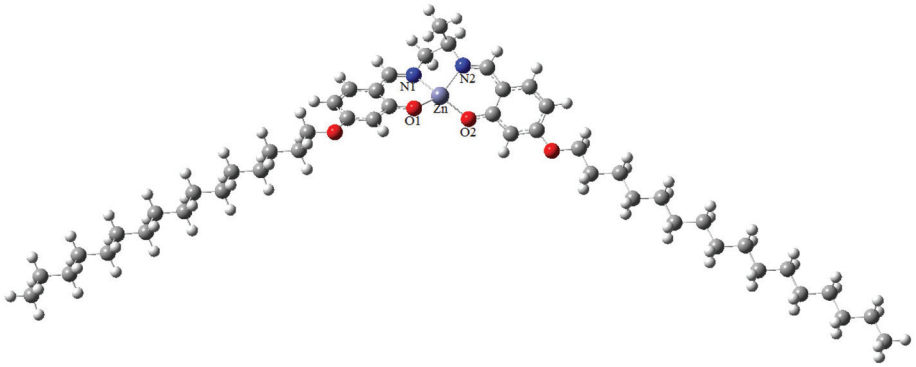

Fig. 8 DFT optimized structure of a representative complex, **Zn-16dap**.

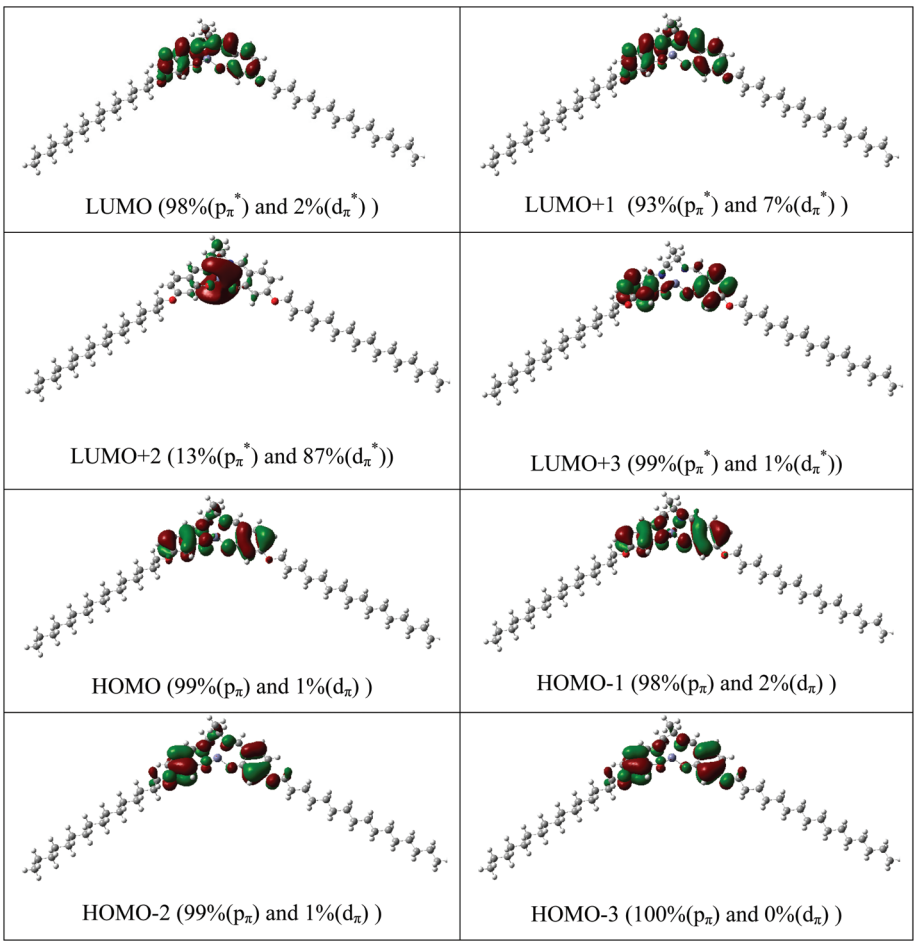

Fig. 9 Frontier molecular orbitals of **Zn-16dap**.

electronic transition. The title complex exhibits three absorption bands at 345, 336 and 295 nm, respectively. The absorption band at 345 nm corresponds to HOMO → LUMO electronic transition owing to the L(π) → L(π*), where HOMO corresponds to π bonding orbitals of aromatic rings of the ligand and LUMO corresponds to π* (anti-bonding) orbitals of the aromatic rings (intra-ligand charge transfer). This transition is consistent with the experimental value of 346 nm. The high energy absorption bands of the complex occur at 336 and 295 nm, which could be assigned to HOMO−1 → LUMO and HOMO−2 → LUMO electronic transitions, predominantly due to intra-ligand (π → π*) charge transfer. These two tran-

Table 5 The experimental absorption bands and the electronic transitions calculated with TD-DFT/B3LYP method of the **Zn-16dap** complex

Key transition	Character	λ (nm)	E (eV)	f (Osc. strength)	Assignments	λ_{exp} (nm) ε (l mol^{-1} cm^{-1})
(90%) HOMO → LUMO	L(π) → L(π^*)	345	3.60	0.124	IL	346 (12 985)
(89%) HOMO−1 → LUMO	L(π) → L(π^*)	336	3.70	0.102	IL	331 (16 998)
(85%) HOMO−2 → LUMO	L(π) → L(π^*)	295	4.21	0.550	IL	286 (29 784)

sitions resemble the experimental value of 331 and 286 nm, respectively.

3. Conclusion

A series of new Zn(II) complexes of 'salen' type asymmetric Schiff base ligands bearing a long pendant alkoxy arm at the 4-position of side aromatic rings and an asymmetric central spacer group have been accessed. Co-ordination of the Zn^{2+} ion to the ligands induces lamello-columnar mesomorphism in otherwise non-mesomorphic ligands. These half-disc shaped molecules assemble in an anti-parallel interdigitated manner within the layer in the mesophase. Metal coordination also brings about interesting fluorescence properties in the solid state, in solution and as well as in the mesophase. In addition, the complexes also exhibit aggregation behaviour in dilute solutions of different non-coordinating and coordinating solvents, suggesting the Lewis acidity of the metal ion in the newly synthesized complexes. Asymmetric methyl substitution at the aliphatic spacer leads to variation in photophysical behaviour and mesophase order in the present complexes as compared to symmetric molecules containing an ethylenediamine spacer. The coordinative unsaturation of Zn(II)-complexes may be utilized for binding with other suitable donor groups to tune the properties.

4. Experimental section

4.1. Physical measurements

The C, H and N analyses were carried out using an Elementar Vario EL III Carlo Erba 1108 elemental analyser. The ^{1}H-NMR spectra were recorded on a Bruker Avance II, 400 MHz spectrometer in $CDCl_3$ (chemical shift in δ) solution with TMS as the internal standard. Ultraviolet-visible absorption spectra of the compounds were recorded on a JASCO V-670 Spectrophotometer. Photoluminescence spectra were recorded on a Perkin Elmer LS 45 Fluorescence Spectrometer. The fluorescence emission quantum yields (EQY) in degassed dichloromethane solutions were determined by the standard optically dilute method[69] using 9,10-diphenylanthracene (EQY = 0.96, in cyclohexane) as the standard.[70] Quantum yield in the solid state was measured by means of an integrating sphere, in which the solid sample film was prepared *via* spin coating and was excited by a 20 kW pulsed xenon source coupled with Monk-Gillieson type monochromators for selecting wavelengths. The resulting luminescence was acquired by an intensified charge-coupled detector for subsequent analyses. Infrared spectra were recorded on a Perkin Elmer BX series spectrometer on KBr disc in the 400–4000 cm^{-1} range. The optical textures of the different phase of the compounds were studied using a Nikon ECLIPSE LV100 POL polarizing microscope attached with Instec hot and cold stage HCS402, with a STC200 temperature controller of 0.1 °C accuracy. The thermal behaviour of the compounds were studied using a Pyris-1 system linked to a Perkin Elmer differential scanning calorimeter (DSC) at a heating or cooling rate of 5 °C min^{-1}. X-ray diffraction (XRD) studies were carried out using samples filled in Lindemann capillaries. The apparatus essentially involved a high-resolution X-ray powder diffractometer (PANalytical X'Pert PRO) equipped with a high-resolution fast detector PIXCEL. Quantum chemical calculation on Zn(II) complex was performed using density functional theory (DFT) as implemented in a GAUSSIAN 09 package.

4.2. Materials

The materials were procured from Tokyo Kasei, Japan and Lancaster Chemicals, USA. All solvents were purified and dried using standard procedures. Silica (60–120 mesh) from Spectrochem was used for chromatographic separation. Silica gel G (E-Merck, India) was used for TLC.

4.3. Synthesis and analysis

4.3.1. Synthesis of *n*-alkoxysalicylaldehyde (*n* = 12, 14, 16). 2,4-Dihydroxybenzaldehyde (10 mmol, 1.38 g), $KHCO_3$ (10 mmol, 1 g), KI (catalytic amount) and 1-bromododecane (10 mmol, 2.4 g) or 1-bromotetradecane (10 mmol, 2.5 g) or 1-bromohexadecane (10 mmol, 2.8 g) were mixed in 250 mL of dry acetone; the mixture was heated under reflux for 24 h, and then filtered, while hot, to remove any insoluble solids. Dilute HCl was added to neutralize the warm solution and then extracted with chloroform (100 mL). The combined chloroform extract was concentrated to give a purple solid. The solid was purified by column chromatography using a mixture of chloroform and hexane (v/v, 1/1) as an eluent. Evaporation of the solvents afforded a white solid product.

4.3.2. Synthesis of *N*,*N*′-bis(4-(4′-*n*-alkoxy)-salicylidene)-1,2-diaminopropane (*n*dap), *n* = 12, 14 or 16

4.3.2.1. General procedure. Schiff bases (***n*dap**) were prepared by adding an ethanolic solution of 2-hydroxy-4-(*n*-alkoxy) salicylaldehyde (1 mmol) to an ethanolic solution of 1,2-diaminopropane (0.5 mmol). The solution mixture was heated under reflux with a few drops of acetic acid as a catalyst for 3 h to yield the light yellow Schiff base, *N*,*N*′-bis(4-(4′-*n*-alkoxy)-

salicylidene)-1,2-diaminopropane. The product was collected by filtration and re-crystallized from absolute ethanol to obtain a pure compound.

4.3.3. *N,N′*-Bis(4-(4′-dodecyloxy)-salicylidene)-1,2-diaminopropane (12dap). Yield = 0.23 g (74%); Anal. Calc. for $C_{41}H_{66}N_2O_4$ (651): C, 75.65; H, 10.22; N, 4.30. Found: C, 75.63; H, 10.21; N, 4.33%. ^{1}H NMR (400 MHz, $CDCl_3$; Me_4Si at 25 °C, ppm): δ = 11.45 (s, 1H, H^7), 8.21 (s, 1H, H^1), 8.17 (s, 1H, $H^{1'}$), 7.01–6.72 (m, 4H, H^2, H^3), 6.21 (s, 2H, H^4), 3.98 (t, $^3J_{H,H}$ = 8 Hz, 4H, O-CH_2), 3.70–3.63 (m, 2H, H^5), 1.68 (m, 3H, H^6), 1.35–1.30 (m, 1H, H^7), 1.22–1.03 (m, –CH_2 of methylene proton in side chain), 0.89 (t, $^3J_{H,H}$ = 8 Hz, 6H, –CH_3). IR (ν_{max}, cm^{-1}, KBr): 3370 (ν_{OH}), 2923 ($\nu_{as(C-H)}$, CH_3), 2857 ($\nu_{s(C-H)}$, CH_3), 1653 ($\nu_{C=N}$), 1227 (ν_{C-O}).

4.3.4. *N,N′*-Bis(4-(4′-tetradecyloxy)-salicylidene)-1,2-diaminopropane (14dap). Yield = 0.29 g (77%); Anal. Calc. for $C_{45}H_{74}N_2O_4$ (707.1): C, 76.44; H, 10.55; N, 3.96. Found: C, 76.47; H, 10.57; N, 3.95%. ^{1}H NMR (400 MHz, $CDCl_3$; Me_4Si at 25 °C, ppm): δ = 11.43 (s, 1H, H^7), 8.23 (s, 1H, H^1), 8.20 (s, 1H, $H^{1'}$), 7.03–6.75 (m, 4H, H^2, H^3), 6.23 (s, 2H, H^4), 3.98 (t, $^3J_{H,H}$ = 8 Hz, 4H, O–CH_2), 3.72–3.65 (m, 2H, H^5), 1.67 (m, 3H, H^6), 1.34–1.27 (m, 1H, H^7), 1.22–1.01 (m, –CH_2 of methylene proton in side chain), 0.89 (t, $^3J_{H,H}$ = 8 Hz, 6H, –CH_3). IR (ν_{max}, cm^{-1}, KBr): 3372 (ν_{OH}), 2922 ($\nu_{as(C-H)}$, CH_3), 2854 ($\nu_{s(C-H)}$, CH_3), 1655 ($\nu_{C=N}$), 1225(ν_{C-O}).

4.3.5. *N,N′*-Bis(4-(4′-hexadecyloxy)-salicylidene)-1,2-diaminopropane (16dap). Yield = 0.31 g (77%); Anal. Calc. for $C_{49}H_{82}N_2O_4$ (763.2): C, 77.11; H, 10.83; N, 3.67. Found: C, 77.13; H, 10.81; N, 3.70%. ^{1}H NMR (400 MHz, $CDCl_3$; Me_4Si at 25 °C, ppm): δ = 11.47 (s, 1H, H^7), 8.22 (s, 1H, H^1), 8.19 (s, 1H, $H^{1'}$), 7.01–6.74 (m, 4H, H^2, H^3), 6.25 (s, 2H, H^4), 3.98 (t, $^3J_{H,H}$ = 8 Hz, 4H, O–CH_2), 3.77–3.58 (m, 2H, H^5), 1.66 (m, 3H, H^6), 1.35–1.28 (m, 1H, H^7), 1.27–1.00 (m, –CH_2 of methylene proton in side chain), 0.88 (t, $^3J_{H,H}$ = 8 Hz, 6H, –CH_3). IR (ν_{max}, cm^{-1}, KBr): 3371(ν_{OH}), 2924 ($\nu_{as(C-H)}$, CH_3), 2856 ($\nu_{s(C-H)}$, CH_3), 1654 ($\nu_{C=N}$), 1225 (ν_{C-O}).

4.3.6. Synthesis of Zinc(II) complexes (Zn-*n*dap, *n* = 12, 14, 16)

4.3.6.1. General procedure. The ligand **12dap** (0.06 g, 0.1 mmol) or **14dap** (0.07 g, 0.1 mmol) or **16dap** (0.08 g, 0.1 mmol) was dissolved in a minimum volume of absolute ethanol. To this, an equimolar amount of zinc acetate $Zn(OAc)_2{\cdot}2H_2O$ (0.02 g, 0.1 mmol) in methanol was then added slowly and stirred for 3 h at room temperature. A white solid formed in each case was filtered, washed with diethyl ether and re-crystallized from chloroform–ethanol (1 : 1).

4.3.7. Zn-12dap. Yield = 0.05 g (75%); Anal. Calc. for $C_{41}H_{64}N_2O_4Zn$ (714.3): C, 68.94; H, 9.03; N, 3.92. Found: C, 68.91; H, 9.07; N, 3.95%. ^{1}H NMR (400 MHz, $CDCl_3$; Me_4Si at 25 °C, ppm): δ = 7.65 (s, 1H, H^1), 7.63 (s, 1H, $H^{1'}$), 6.97–6.70 (m, 4H, H^2, H^3), 6.26 (s, 2H, H^4), 3.99 (t, $^3J_{H,H}$ = 8 Hz, 4H, O–CH_2), 3.73–3.67 (m, 2H, H^5), 1.65 (m, 3H, H^6), 1.36–1.31 (m, 1H, H^7), 1.26–0.99 (m, –CH_2 of methylene proton in side chain), 0.88 (t, $^3J_{H,H}$ = 8 Hz, 6H, –CH_3). IR (ν_{max}, cm^{-1}, KBr): 2919 ($\nu_{as(C-H)}$, CH_3), 2853 ($\nu_{s(C-H)}$, CH_3), 1639 ($\nu_{C=N}$), 1215 (ν_{C-O}).

4.3.8. Zn-14dap. Yield = 0.06 g (78%); Anal. Calc. for $C_{45}H_{72}N_2O_4Zn$ (770.5): C, 70.15; H, 9.42; N, 3.64. Found: C, 70.14; H, 9.45; N, 3.65%. ^{1}H NMR (400 MHz, $CDCl_3$; Me_4Si at 25 °C, ppm): δ = 7.68 (s, 1H, H^1), 7.66 (s, 1H, $H^{1'}$), 6.99–6.71 (m, 4H, H^2, H^3), 6.27 (s, 2H, H^4), 3.99 (t, $^3J_{H,H}$ = 8 Hz, 4H, O–CH_2), 3.76–3.60 (m, 2H, H^5), 1.70 (m, 3H, H^6), 1.37–1.26 (m, 1H, H^7), 1.27–1.07 (m, –CH_2 of methylene proton in side chain), 0.89 (t, $^3J_{H,H}$ = 8 Hz, 6H, –CH_3). IR (ν_{max}, cm^{-1}, KBr): 2921 ($\nu_{as(C-H)}$, CH_3), 2856 ($\nu_{s(C-H)}$, CH_3), 1639 ($\nu_{C=N}$), 1217 (ν_{C-O}).

4.3.9. Zn-16dap. Yield = 0.06 g (77%); Anal. Calc. for $C_{49}H_{80}N_2O_4Zn$ (826.6): C, 71.20; H, 9.76; N, 3.39. Found: C, 71.17; H, 9.78; N, 3.40%. ^{1}H NMR (400 MHz, $CDCl_3$; Me_4Si at 25 °C, ppm): δ = 7.67 (s, 1H, H^1), 7.64 (s, 1H, $H^{1'}$), 7.00–6.73 (m, 4H, H^2, H^3), 6.22 (s, 2H, H^4), 3.99 (t, $^3J_{H,H}$ = 8 Hz, 4H, O–CH_2), 3.74–3.60 (m, 2H, H^5), 1.64 (m, 3H, H^6), 1.34–1.24 (m, 1H, H^7), 1.28–0.98 (m, –CH_2 of methylene proton in side chain), 0.87 (t, $^3J_{H,H}$ = 8 Hz, 6H, –CH_3). IR (ν_{max}, cm^{-1}, KBr): 2917 ($\nu_{as(C-H)}$, CH_3), 2854 ($\nu_{s(C-H)}$, CH_3), 1637 ($\nu_{C=N}$), 1215 (ν_{C-O}).

Acknowledgements

SC and PM acknowledge the Department of Science and Technology (DST), New Delhi, Government of India for the INSPIRE Junior Research Fellowship (Code: IF110692) and financial support (SR/FT/CS-86/2010), respectively. Sophisticated Analytical Instrumentation Facility (SAIF), North Eastern Hill University, Shillong and Central Drug Research Institute (CDRI), Lucknow are acknowledged for some spectral results. The authors are also thankful to DBT e-Library Consortium (DeLCON) of Bio-Informatics Centre, Assam University, India.

References

1 A. W. Kleij, *Eur. J. Inorg. Chem.*, 2009, 193–205.
2 A. W. Kleij, *Chem. – Eur. J.*, 2008, **14**, 10520–10529.
3 S. J. Wezenberg and A. W. Kleij, *Angew. Chem., Int. Ed.*, 2008, **47**, 2354–2364.
4 G. H. Clever and T. Carell, *Angew. Chem., Int. Ed.*, 2007, **46**, 250–253.
5 K. C. Gupta and A. K. Sutar, *Coord. Chem. Rev.*, 2008, **252**, 1420–1450.
6 P. G. Cozzi, *Chem. Soc. Rev.*, 2004, **33**, 410–421.
7 L. Canali and D. C. Sherrington, *Chem. Soc. Rev.*, 1999, **28**, 85–93.
8 E. N. Jacobsen, in *Catalytic Asymmetric Synthesis*, ed. I. Ojima, VCH, New York, 1993, p. 159.
9 G. Barone, N. Gambino, A. Ruggirello, A. Silvestri, A. Terenzi and V. T. Liveri, *J. Inorg. Biochem.*, 2009, **103**, 731–737.
10 Y. Kou, J. Tian, D. Li, W. Gu, X. Liu, S. Yan, D. Liao and P. Cheng, *Dalton Trans.*, 2009, 2374–2382.

11 A. Silvestri, G. Barone, G. Ruisi, D. Anselmo, S. Riela and V. T. Liveri, *J. Inorg. Biochem.*, 2007, **101**, 841–848.
12 C. Liu, M. Wang, T. Zhang and H. Sun, *Coord. Chem. Rev.*, 2004, **248**, 147–168.
13 J. Cheng, K. Wei, X. Ma, X. Zhou and H. Xiang, *J. Phys. Chem. C*, 2013, **117**, 16552–16563.
14 V. Liuzzo, W. Oberhauser and A. Pucci, *Inorg. Chem. Commun.*, 2010, **13**, 686–688.
15 H.-C. Lin, C.-C. Huang, C.-H. Shi, Y.-H. Liao, C.-C. Chen, Y.-C. Lin and Y.-H. Liu, *Dalton Trans.*, 2007, 781–791.
16 E. Hadjoudis and I. M. Mavridis, *Chem. Soc. Rev.*, 2004, **33**, 579–588.
17 M. Andruh, *Chem. Commun.*, 2011, **47**, 3025–3042.
18 H. Miyasaka, A. Saitoh and S. Abe, *Coord. Chem. Rev.*, 2007, **251**, 2622–2664.
19 I. P. Oliveri, S. Failla, A. Columbo, C. Dragonetti, S. Righetto and S. Di Bella, *Dalton Trans.*, 2014, **43**, 2168–2175.
20 S. Di Bella, I. P. Oliveri, A. Colombo, C. Dragonetti, S. Righetto and D. Roberto, *Dalton Trans.*, 2012, **41**, 7013–7016.
21 P. G. Lacroix, *Eur. J. Inorg. Chem.*, 2001, 339–348.
22 C. Datta, R. Chakrabarty, G. Das, C. R. Bhattacharjee and P. Mondal, *Liq. Cryst.*, 2013, **41**, 541–551.
23 C. R. Bhattacharjee, C. Datta, G. Das, R. Chakrabarty and P. Mondal, *Polyhedron*, 2012, **33**, 417–424.
24 Y. Abe, Y. Takagi, M. Nakamura, T. Takeuchi, T. Tanase, M. Yokokawa, H. Mukai, T. Megumi, A. Hachisuga and K. Ohta, *Inorg. Chim. Acta*, 2012, **392**, 254–260.
25 A. Ohta, Y. Yamamoto, H. Kamihata, Y. H. Lee, F. Ichikawa, K. Ohta, Y. Abe, N. Hoshino, M. Kojima and S. Hayami, *Inorg. Chem. Commun.*, 2012, **16**, 89–91.
26 C. R. Bhattacharjee, G. Das, P. Mondal, S. K. Prasad and D. S. S. Rao, *Inorg. Chem. Commun.*, 2011, **14**, 606–612.
27 Y. Abe, N. Nakazima, T. Tanase, S. Katano, H. Mukai and K. Ohta, *Mol. Cryst. Liq. Cryst.*, 2007, **466**, 129–147.
28 Y. Abe, K. Nakabayashi, N. Matsukawa, H. Takashima, M. Iida, T. Tanase, M. Sugibayashi, H. Mukai and K. Ohta, *Inorg. Chim. Acta*, 2006, **359**, 3934–3946.
29 K. Binnemans, K. Lodewyckx, T. Cardinaes, T. N. Parac Vogt, C. Bourgogne, D. Guillon and B. Donnio, *Eur. J. Inorg. Chem.*, 2006, 150–157.
30 Y. Abe, H. Akao, Y. Yoshida, H. Takashima, T. Tanase, H. Mukai and K. Ohta, *Inorg. Chim. Acta*, 2006, **359**, 3147–3155.
31 L. L. Li, H. F. Xiang, X. G. Zhou, M. L. Li and D. Wu, *J. Chem. Educ.*, 2012, **89**, 559–560.
32 V. K. Gupta, R. N. Goyal, A. K. Jain and R. A. Sharma, *Electrochim. Acta*, 2009, **54**, 3218–3224.
33 V. K. Gupta, A. K. Jain and G. Maheshwari, *Talanta*, 2007, **72**, 49–53.
34 D. Pucci, I. Aiello, A. Bellusci, A. Crispini, M. Ghedini and M. La Deda, *Eur. J. Inorg. Chem.*, 2009, 4274–4281.
35 C. R. Bhattacharjee, S. Chakraborty, G. Das and P. Mondal, *Liq. Cryst.*, 2012, **39**, 1435–1442.
36 C. R. Bhattacharjee, G. Das, P. Mondal, S. K. Prasad and D. S. S. Rao, *Eur. J. Inorg. Chem.*, 2011, 1418–1424.
37 C. R. Bhattacharjee, G. Das, P. Mondal and N. V. S. Rao, *Polyhedron*, 2010, **29**, 3089–3096.
38 I. P. Oliveri and S. Di Bella, *Tetrahedron*, 2011, **67**, 9446–9449.
39 M. E. Germain and M. J. Knapp, *J. Am. Chem. Soc.*, 2008, **130**, 5422–5423.
40 M. E. Germain, T. R. Vargo, P. G. Khalifah and M. J. Knapp, *Inorg. Chem.*, 2007, **46**, 4422–4429.
41 M. Cano, L. Rodríguez, J. C. Lima, F. Pina, A. D. Cort, C. Pasquini and L. Schiaffino, *Inorg. Chem.*, 2009, **48**, 6229–6235.
42 A. D. Cort, L. Mandolini, C. Pasquini, K. Rissanen, L. Russo and L. Schiaffino, *New J. Chem.*, 2007, **31**, 1633–1638.
43 S. J. Wezenberg, E. C. Escudero-Adán, J. Benet-Buchholz and A. W. Kleij, *Inorg. Chem.*, 2008, **47**, 2925–2927.
44 A. W. Kleij, M. Kuil, D. M. Tooke, A. L. Spek and J. N. H. Reek, *Inorg. Chem.*, 2007, **46**, 5829–5831.
45 M. Kuil, I. M. Puijk, A. W. Kleij, D. M. Tooke, A. L. Spek and J. N. H. Reek, *Chem. – Asian J.*, 2009, **4**, 50–57.
46 A. W. Kleij, M. Kuil, D. M. Tooke, M. Lutz, A. L. Spek and J. N. H. Reek, *Chem. – Eur. J.*, 2005, **11**, 4743–4750.
47 M. Kuil, P. E. Goudriaan, A. W. Kleij, D. M. Tooke, A. L. Spek, P. W. N. M. van Leeuwen and J. N. H. Reek, *Dalton Trans.*, 2007, 2311–2320.
48 P. G. Cozzi, *Angew. Chem., Int. Ed.*, 2003, **115**, 3001–3004.
49 A. A. Vashchenko, L. S. Lepnev, A. G. Vitukhnovskii, O. V. Kotova, S. V. Eliseeva and N. P. Kuz'mina, *Opt. Spectrosc.*, 2010, **108**, 463–465.
50 O. V. Kotova, S. V. Eliseeva, A. S. Averjushkin, L. S. Lepnev, A. A. Vaschenko, A. Y. Rogachev, A. G. Vitukhnovskii and N. P. Kuzmina, *Russ. Chem. Bull. Int. Ed.*, 2008, **57**, 1880–1889.
51 K. H. Chang, C. C. Huang, Y. H. Liu, Y. H. Hu, P. T. Chou and Y. C. Lin, *Dalton Trans.*, 2004, 1731–1738.
52 G. Consiglio, S. Failla, P. Finocchiaro, I. P. Oliveri and S. Di Bella, *Inorg. Chem.*, 2012, **51**, 8409–8418.
53 G. Consiglio, S. Failla, P. Finocchiaro, I. P. Oliveri and S. Di Bella, *Dalton Trans.*, 2012, **41**, 387–395.
54 G. Consiglio, S. Failla, I. P. Oliveri, R. Purrello and S. Di Bella, *Dalton Trans.*, 2009, 10426–10428.
55 A. W. Kleij, *Dalton Trans.*, 2009, 4635–4639.
56 A. G. Serrette, C. K. Lai and T. M. Swager, *Chem. Mater.*, 1994, **6**, 2252–2268.
57 S. T. Trzaska and T. M. Swager, *Chem. Mater.*, 1998, **10**, 438–443.
58 H.-C. Lin, C.-C. Huang, C.-H. Shi, Y.-H. Liao, C.-C. Chen, Y.-C. Lin and Y.-H. Liu, *Dalton Trans.*, 2007, 781–791.
59 M. Kasha, H. R. Rawls and M. A. El-Bayoumi, *Pure Appl. Chem.*, 1965, **11**, 371–392.
60 G. E. Batley and D. P. Graddon, *Aust. J. Chem.*, 1967, **20**, 885–891.
61 S. Mizukami, H. Houjou, Y. Nagawa and M. Kanesato, *Chem. Commun.*, 2003, 1148–1149.

62 M. J. Frisch, G. W. Trucks, H. B. Schlegel, G. E. Scuseria, M. A. Robb, J. R. Cheeseman, G. Scalmani, V. Barone, B. Mennucci, G. A. Petersson, H. Nakatsuji, M. Caricato, X. Li, H. P. Hratchian, A. F. Izmaylov, J. Bloino, G. Zheng, J. L. Sonnenberg, M. Hada, M. Ehara, K. Toyota, R. Fukuda, J. Hasegawa, M. Ishida, T. Nakajima, Y. Honda, O. Kitao, H. Nakai, T. Vreven, J. A. Montgomery Jr., J. E. Peralta, F. Ogliaro, M. Bearpark, J. J. Heyd, E. Brothers, K. N. Kudin, V. N. Staroverov, R. Kobayashi, J. Normand, K. Raghavachari, A. Rendell, J. C. Burant, S. S. Iyengar, J. Tomasi, M. Cossi, N. Rega, J. M. Millam, M. Klene, J. E. Knox, J. B. Cross, V. Bakken, C. Adamo, J. Jaramillo, R. Gomperts, R. E. Stratmann, O. Yazyev, A. J. Austin, R. Cammi, C. Pomelli, J. W. Ochterski, R. L. Martin, K. Morokuma, V. G. Zakrzewski, G. A. Voth, P. Salvador, J. J. Dannenberg, S. Dapprich, A. D. Daniels, Ö. Farkas, J. B. Foresman, J. V. Ortiz, J. Cioslowski and D. J. Fox, *Gaussian 09*, Gaussian, Inc., Wallingford, CT, 2009.
63 A. D. Becke, *J. Chem. Phys.*, 1993, **98**, 5648–5652.
64 C. Lee, W. Yang and R. G. Parr, *Phys. Rev. B: Condens. Matter*, 1988, **37**, 785–789.
65 P. C. Hariharan and J. A. Pople, *Theor. Chim. Acta*, 1973, **28**, 213–222.
66 N. M. O'Boyle, A. L. Tenderholt and K. M. Langner, *J. Comput. Chem.*, 2008, **29**, 839–845.
67 E. Cance, B. Mennucci and J. Tomasi, *J. Chem. Phys.*, 1997, **107**, 3032–3041.
68 S. Miertus, E. Scrocco and J. Tomasi, *J. Chem. Phys.*, 1981, **55**, 117–129.
69 J. N. Demas and G. A. Crosby, *J. Phys. Chem.*, 1971, **75**, 991–1024.
70 W. R. Ware and W. Rothman, *Chem. Phys. Lett.*, 1976, **39**, 449–453.